

Self-distillation Augmented Masked Autoencoders for Histopathological Image Classification

Yang Luo¹, Zhineng Chen¹, and Xieping Gao²

¹Fudan University, Shanghai, China

²Hunan Provincial Key Laboratory of Intelligent Computing and Language Information Processing, Hunan Normal University
yangluo21@m.fudan.edu.cn

Abstract. Self-supervised learning (SSL) has drawn increasing attention in pathological image analysis in recent years. Compared to contrastive learning which requires careful design, masked autoencoders (MAE) building SSL from a generative paradigm probably is a simpler method. In this paper, we introduce MAE and verify the effect of visible patches for pathological image classification. Based on it, a novel SD-MAE model is proposed to enable a self-distillation augmented SSL on top of the raw MAE. Besides the reconstruction loss on masked image patches, SD-MAE further imposes the self-distillation loss on visible patches. It transfers knowledge brought by the global attention of the decoder to the encoder which only uses local attention. We apply SD-MAE on two public pathological image datasets. Experiments demonstrate that SD-MAE performs highly competitive when compared with other SSL methods. Our code will be released soon.

Keywords: Self-supervised learning · MAE · Self distillation.

1 Introduction

With the advancement of deep learning, self-supervised learning (SSL) has received increasing research attention [9,7,11,6]. SSL is a special unsupervised learning that learns the image representation by using different input sensor signals to automatically label training data, i.e., pretext task [15]. A number of practices [10,5,1] show that such a paradigm can establish an effective feature pre-training for downstream tasks. Furthermore, SSL is particularly suitable for medical image analysis, as supervised learning still remains the dominating technique for many medical image analysis tasks so far, which, however, relies heavily on time-consuming manual annotations. For histopathological images, Typical examples include predicting cube rotation of 3D medical images [27], leveraging nuclei size and quantity to extract the instance-aware feature [22], or solving jigsaw puzzles [18] and so on. Self-supervised contrastive learning is perhaps the most prevalent SSL paradigm in the past few years [5,7,6]. It aims to learn representations that maximize the agreement between different views, and simultaneously minimize the similarity between two unrelated

instances. Generally, different views are augmentations from the same instance. Although several studies [25,20,8] have successfully applied self-supervised contrastive learning to different pathological image analysis tasks, Stacke *et al* [17] argue that this paradigm not only needs careful design but also might be suboptimal. The reason mainly comes from two aspects. First, different pathological image regions are somewhat homogeneous, i.e., their visual appearances are similar, although they are labeled as different categories such as normal and tumor, or normal, situ, invasive, etc., for different clinical purposes. Consequently, it is not easy to extract informative positives. Second, due to the fact that datasets of pathological image classification are typical few, e.g., 2 or 4 [24,2], contractive learning might suffer a problem of false negatives. More specifically, the learning procedure has a larger risk of pushing away two images, despite that they belong to the same category, i.e., normal.

Recently, He *et al.* [11] proposed a new SSL paradigm termed masked autoencoders (MAE). It falls into the transformer-based encoder-decoder framework, but the two sides are asymmetric. Image reconstruction [16] is used as the pre-text task which formulates the learning in a generative way. Concretely, the task uses a few visible image patches to reconstruct the other masked patches. When the training is finished, the decoder is dispensed while the learned encoder establishes a pre-trained backbone for downstream tasks. This paradigm has the advantages of not being affected by the category number. It thus more friendly to the pathological image analysis. However, it is observed that there is no work using MAE to analyze pathological images now.

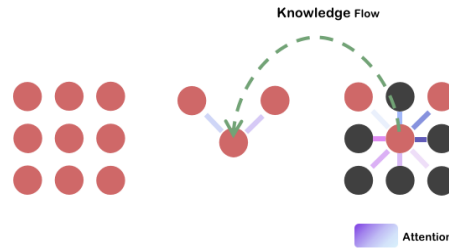


Fig. 1. Intuition graph for SD-MAE. The dots represent patches of an image (red ones are visible patches, and blank ones are masked patches). And pictures from left to right are raw image, visible patches in the encoder, and the all patches in the decoder. We leverage the advantage of global attention of visible patches in the decoder, regard this global information as knowledge, and thus transfer this knowledge from the decoder to the encoder.

Motivated by the analysis above, we want to introduce MAE to pathological image analysis. And we observe that MAE only imposes constraints on reconstructed masked patches, i.e., requiring them as similar as the raw ones, but ignores the effect of visible patches. And we find these visible patches have the potential, if applied correctly, to improve performance of the encoder for patho-

logical image classification (see Sec. 2.2). Based on it, we develop SD-MAE, a self-distillation augmented MAE which enables a self-distillation augmented SSL on top of the raw MAE. As shown in Fig. 1, the encoder leverage local attention, which restrains each visible patch to only interact with other visible ones, to extract the feature. And yet the decoder leverage global attention, which allows each patch to interact with all the ones, to reconstruct the masked patches. We argue that the visible patches in the decoder contain **more** knowledge compared with ones in the encoder, and thus we can transfer this knowledge from the decoder to the encoder. Specifically, the feature vectors of the visible patches obtained from the encoder are treated as the student while their counterpart from the decoder as the teacher. Therefore, imposing additional constraints on the two kinds of features is conducive to improving the abstraction of feature obtained from the encoder, and subsequently, leading to a more powerful feature representation. We implement this idea and carry out image classification experiments on two pathological. It is shown that SD-MAE gains highly competitive results when compared with leading contrastive-based SSL methods. Moreover, the results of visualization also show self-distillation could enable the encoder to be more focused (see Sec. 3.5 and Fig. 4). Our contributions can be summarized as follows:

- We thoroughly analyzed the effect of visible patches and design experiments to verify that we can leverage them to enhance the MAE encoder by decoupling MSE loss in pathological image classification.
- Benefiting from the above finding, we proposed SD-MAE, a self-distillation augmented MAE. It has the advantages of enhancing the feature representation on top of MAE, thus further benefiting downstream tasks.
- We carry out experiments on two pathological image datasets and visualization results, which basically verifies that SD-MAE generates a more effective feature representation and improves the image classification accuracy

2 Methodology

An illustrative framework of the proposed SD-MAE is shown in Fig. 2. It has two modules, i.e., masked image modeling and visible image modeling. The former aims to enable a generative SSL on unlabeled data by constraining the masked image patches, while the latter further imposes self-distillation constraints on visible patches to guide a more effective encoder learning. It is an elegant complementary to the raw MAE especially for pathological images. We will introduce the modules as follows.

2.1 Masked Image Modeling

MAE [11] is leveraged as our masked image modeling block. Its modeling process is independent of the category number, thus more friendly to pathological image analysis. Generally, it consists of four components:

Patchifying and Masking decides how to mask the input images and the masking ratio. For patchifying, the input image $x \subseteq \mathbb{R}^{H \times W \times C}$ is firstly extracted by convolutions with kernel size (P, P) and stride P into N patches, where $N = HW/P^2$. The size of each patch is $\frac{H}{P} \times \frac{W}{P} \times C$. Then, each patch is flattened to a token, i.e., a 1-dimensional vector of visual feature with length $D = P^2C$. The representation of all patches is formulated as $v_{all} \subseteq \mathbb{R}^{N \times D}$. For masking, we randomly divide patches into two sets according to a masking ratio m , namely $v_{all} \subseteq \mathbb{R}^{N \times D} \rightarrow v_{vis} \subseteq \mathbb{R}^{N' \times D}, v_m \subseteq \mathbb{R}^{\tilde{N}' \times D}$ where $N' = N*(1-m), \tilde{N}' = N*m$. v_{vis} will be used as the input of encoder and v_m as the labels.

Encoder takes v_{vis} as input, and extract latent feature from *visible patches*. Unlike convolution, ViT is suitable for MAE due to its "isotropic" architecture [19] whose size and shape of the output is equal to the input. The encoder firstly maps D dimensions of tokens to D' with a trainable linear projection, and adds holistic positional embeddings to the visible tokens, that is $z_{vis} = E_{pos} + v'$, where $E_{pos} \subseteq \mathbb{R}^{N' \times D'}$, and then processes z_{vis} via a series of Transformer blocks, getting latent representation vectors of patches $z'_{vis} \subseteq \mathbb{R}^{N' \times D'}$.

Decoder impels masked tokens $z_m \subseteq \mathbb{R}^{\tilde{N}' \times D'}$ to learn low-level representation from visible patches for subsequent image reconstruction. Initially, the decoder concatenates z'_{vis} and z_m as one matrix $z_{all} \subseteq \mathbb{R}^{N \times D'}$. For keeping the positional relation of patches, Decoder also adds positional embeddings to all patches $z'_{all} = E'_{pos} + v'$, where $E'_{pos} \subseteq \mathbb{R}^{N \times D'}$. The full set of tokens are processed via decoder. As a result, $y_{all} \subseteq \mathbb{R}^{N \times D'}$, the decoder output was divide into y_{vis} and y_m , indicating visible and masked tokens respectively.

Prediction target defines how to predict the original signals. Before predicting, we consider the original masked tokens after normalizing $Y_m = Norm(v_m)$ are our prediction target. The decoder will use a linear layer to align y_m and Y , namely $y_m \rightarrow y'_m$. We compute the mean square error (MSE) loss between the predicted y'_m and labels Y_m .

$$L_{mse} = MSE(y'_m, Y_m) \quad y'_m, Y_m \subseteq \mathbb{R}^{\tilde{N}' \times D} \quad (1)$$

2.2 Rethinking Visible Patches

The experiment of [11,23] show that simply computed on the whole image (both visible tokens and masked tokens) could be harmful on ImageNet dataset. For exploring the effect of visible tokens, we delve into the design of loss function. We reformulate the original MSE loss into a weighted sum of two parts, one is relevant to the masked tokens, and the other is visible tokens. We name this deformation as decoupling.

Specifically, the original MAE only predict on masked tokens, as shown in Eq.(1). And we can easily get the loss function computed at full patches:

$$L_{mse} = MSE(y'_m + y'_v, Y_m + Y_v) \quad (2)$$

where y'_v and Y'_v are the prediction and the label of visible tokens, respectively. Then, Eq. (2) can be rewritten as:

$$L_{mse} = MSE(y'_m, Y_m) + MSE(y'_v, Y_v) \quad (3)$$

One reason of why the original MAE do not use a loss among the visible patches is that all the information from the visible tokens can be explicitly “sprinkled” in the masked tokens by self-attention layers and can be recovered easily during the decoding stage. But it is these visible patches that the encoder extract features from, and it is this encoder which is actually the part we need in down-stream tasks. Consequently, we agree that if these patches are directly added to the calculation of the loss rather than being "sprinkled" in the masked tokens, this will improve the ability of extracting features of the encoder by backpropagation. We also could explain this from visualization of attention map (see Sec. 3.5). But because of the mask ratio (a very high ratio), we can not simply use equal proportion to calculate visible patches and masked patches in the loss function.

So we can rewrite Eq. (3) as:

$$L_{mse} = p * MSE(y'_v, Y_v) + (1 - p) * MSE(y'_m, Y_m) \quad (4)$$

The loss is reformulated into a weighted sum of two terms. And we introduce a hyperparameter p as the weight of visible patches. We designed a series of experiments under different conditions (see Tab. 1) to verify its effectiveness and universality. As shown in Tab. 2, we could clearly find that decoupling, in most cases, is better than or comparable to the MSE loss only computed at masked patches for pathological image classification (see green results in Tab. 2).

With this result, we can empirically conclude that we can leverage visible patches to enhance the encoder. Moreover, Zhang *et al.* [26] introduce self distillation to squeeze the knowledge of deeper layer into the shallow ones within a network. Inspired by it, we propose a novel self-distillation method to transfer knowledge from visible patches after decoding to the encoder.

Table 1. Considering the size of model and weight updating are two key factors of training, these conditions are applied to prove the effectiveness of the decoupling.

ID	Arch.	Param.	Pre-training	Fine-tuning	
			Learning rate	Learning rate	Weigh-decay
S1	ViT-S	21	1e-4	5e-4	5e-3
S2	ViT-S	21	1e-4	5e-4	5e-2
S3	ViT-S	21	1.5e-4	5e-4	5e-2
S4	ViT-S	21	1.5e-4	1e-3	5e-2
T1	ViT-T	5	1.5e-4	1e-3	5e-2

Table 2. The top-1 accuracy of different experiments on the three datasets. M, F, P0.1, P0.2 and P0.3 denotes calculating MSE loss on masked patches, on full patches, decoupling with $p = 0.1$, decoupling with $p = 0.2$ and decoupling with $p = 0.3$.

ID	PCam					NCT-CRC					MSSvsMSI				
	M	F	P0.1	P0.2	P0.3	M	F	P0.1	P0.2	P0.3	M	F	P0.1	P0.2	P0.3
S1	87.6	86.5	89.1	88.4	88.9	94.1	93.8	94.5	94.1	94.2	92.8	92.5	93.6	93.4	93.3
S2	87.1	86.7	86.6	87.7	88.2	94.5	94.2	94.3	94.3	94.4	93.0	93.1	94.0	93.5	93.5
S3	88.2	88.7	88.3	88.1	88.0	94.7	94.2	93.9	93.8	94.7	95.0	95.2	95.2	95.6	95.7
S4	87.8	87.1	88.0	88.1	85.8	94.7	95.3	94.6	94.1	94.4	94.6	94.0	94.6	94.4	94.3
T1	85.2	86.2	87.5	86.8	85.4	94.1	93.8	93.9	93.9	94.2	90.6	87.1	89.4	89.4	88.7

2.3 Self-Distillation Augmented Visible Patches

Knowledge Distillation is a wide method that reinforces the learning capability of the student model by transferring knowledge from the teacher model [12]. Usually the teacher model is a large capacity network while the student model is a small network. In addition, Zhang *et al.* [26] firstly apply it to the vectors at different depths within the same neural network. It distills knowledge from deeper layers to shallow layers, enhancing the feature representation of shallow layers. And considering the imbalance of knowledge (see Sec. 1), we found that this is exactly how knowledge in the visible tokens can be transferred from the decoder to the encoder through this distillation paradigm. Specifically, there are two kinds of latent representation vectors for visible tokens in MAE, namely z'_{vis} after encoding and y_{vis} after decoding. We treat them either as shallow and deep features in the self-distillation framework [26]. We use a 3-layer MLP over these two vectors, resulting in two high-dimension q and p , respectively. We further regard $Softmax(q)$ as probability distribution of discrete visible patches in hidden space, and $Softmax(p)$ as labels of these visible patches. Therefore, we learn to match these two distributions by minimizing the cross-entropy loss, which can be described as follows:

$$\begin{aligned}
 q &= MLP(z'_{vis}), \quad p = MLP(y_{vis}) \\
 q' &= Softmax(q), \quad p' = Softmax(p) \\
 L_{distill} &= -p' \log(q')
 \end{aligned} \tag{5}$$

The total loss is formulated as follows:

$$L = L_{mse} * \alpha + L_{distill} * (1 - \alpha) \tag{6}$$

where α is the empirically determined scaling factor (in our work $\alpha = 0.2$).

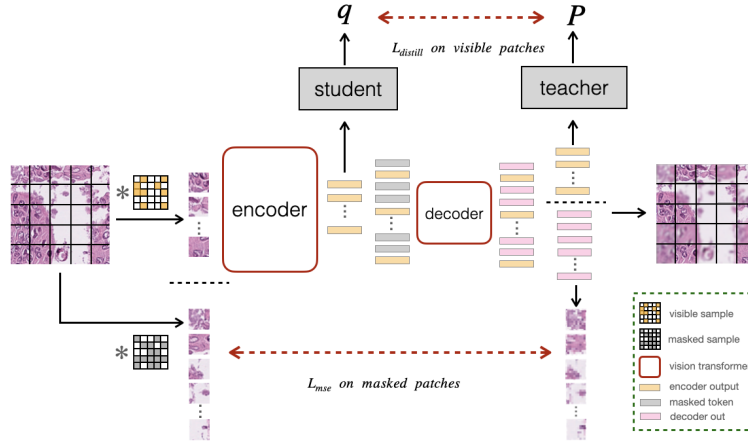


Fig. 2. Illustrative framework of the proposed SD-MAE. Besides the raw MAE, we make use of visible patches after decoding and apply them as the teacher to transfer knowledge to their counterparts after encoding.

3 Experiments

3.1 Datasets

To evaluate its effectiveness, we train our SD-MAE on two public pathological image datasets (i.e., PatchCamelyon, NCT-CRC-HE). Their details are as follows.

PatchCamelyon. PatchCamelyon(PCam) [3] consists of 327,680 96×96 color images extracted from Camelyon16 dataset [4]. Each image is labeled as either normal or tumor. There are 262,144, 32,768 and 32,768 for training, validation and test. We use training dataset for self-supervised learning, and use training dataset and validation dataset for fine-tuning learning. And the accuracy on the test set is reported as the evaluation metric.

MSIvsMSS. MSIvsMSS [13] is a dataset derived from colorectal cancer and gastric cancer patients in the TCGA cohort, and contains 192,312 224×224 images. Each image is labeled as either MSI (microsatellite instable or highly mutated) or MSS (microsatellite stable). There are 153,851 and 38,461 for training and validation. We apply the accuracy on the validation set as the evaluation metric we report.

NCT-CRC-HE. NCT-CRC-HE(NCT-CRC) [14] is a dataset manually extracted from H&E stained human colorectal cancer images. Its tissues are divided into eight classes of colorectal cancer and one class of normal tissue. It contains 89,343 and 6,333 224×224 images for training and validation, respectively. Following [25,20], we exclude images belonging to the background in both training and validation set. The evaluation metric we report is similar to the MSSvsMSS.

Table 3. End-to-end fine-tuning evaluation results on PCam and NCT-CRC. * are run by us.

Methods	Arch.	Param.	Datasets and Metrics				
			PatchCamelyon			NCT-CRC	
			F1-score	Acc	AUC	F1-score	Acc
Supervised	ViT-S	21	79.2± 2.9	79.8± 2.6	93.1± 0.6	89.6± 0.3	92.1± 0.6
CS-CO	ResNet18	22	-	-	-	89.0± 0.3	91.4± 0.3
TransPath*	ViT-S	21	81.0± 1.3	81.2± 1.2	91.7± 0.4	89.9± 0.6	92.8± 0.8
MoCo v3*	ViT-S	21	86.2± 2.3	86.3± 2.2	95.0± 0.6	92.6± 0.4	94.4± 0.4
DINO*	ViT-S	21	85.6± 0.6	85.8± 0.5	95.7± 0.3	91.6± 0.6	94.4± 0.1
MAE*	ViT-S	21	86.2± 1.0	86.7± 1.3	95.8± 0.3	92.4± 1.0	94.7± 0.5
SD-MAE	ViT-S	21	87.8± 0.8	88.2± 0.5	96.2± 0.2	93.5± 1.0	95.3 ± 0.4

3.2 Experimental Setup

We follow almost the same protocol in MAE [11] to train our SD-MAE. The input images are resized to 224 x 224 and the batch size is set 1024 in both pre-training and fine-tuning steps. We split images into 14×14 patches with size of 16 x 16. The same as most generative methods, *RandomResizedCrop* is the only augmentation strategy in pre-training. The same as [7,23,11,21,25], both pre-training and fine-tuning are carried out on the same dataset.

We use ViT-S (12 transformer blocks with dimension 384) as the encoder and employ a lightweight decoder (4 transformer blocks with dimension 192 and a linear projection for patch recovering). In pre-training, the masking ratio is 0.6 (a relative small masking ratio reports the best accuracy according to our ablation study). We apply L2-normalization bottleneck [5] (dimension 256 and 4096 for the bottleneck and the hidden dimension, respectively) as the projection head in self-distillation. Our SD-MAE adopt 100-epoch training and 5-epoch warm-up. All the experiments are carried out on Pytorch with 4 Nvidia 3090 GPUs.

For a fair comparison, we use the respective pre-training methods to train the models [5,7,20,11], and then use a unified approach [11] to fine-tune them.

3.3 Results and Comparisons

Tab. 3 list the accuracy of different methods on the two datasets. As a baseline, ViT-S is directly trained using the dataset without SSL-based pre-training, thus representing a metric whether SSL takes effect. As for the results of the two self-supervised learning methods for pathological image classification. CS-CO reports a result even worse than ViT-S. It is explained as the difference between the network capacity, where double ResNet-18 is employed as the backbone in CS-CO. And we find that MoCo v3 as a classical contrastive learning method has high standard deviation when the dataset has fewer classes. The results demonstrate that contrastive methods, although have potential, require careful design based on the dataset to get good results, but this is difficult to satisfy in pathological images [17]. DINO is more stable by using cross-entropy instead of InfoNCE loss. As a comparison, the way MAE uses image reconstruction

is obviously more friendly for pathological images. In contrast, our SD-MAE shows steady improvements over MAE on the two datasets, especially for binary classification. It implies that self-distillation extracts feature complementary to the reconstruction task in MAE. We will verify our hypothesis in the near future.

3.4 Transfer Learning

Table 4. Main transfer results with different pre-train data

Method	Pre-train data			Fine-tune data			Acc
	PCam	MSIvsMSS	NCT-CRC	PCam	MSIvsMSS	NCT-CRC	
MAE							87.2
SD-MAE	✓				✓		91.2
MAE							90.2
SD-MAE		✓		✓			90.3
MAE							88.5
SD-MAE			✓	✓			89.7
MAE							89.1
SD-MAE			✓		✓		90.3
MAE	✓					✓	93.8
SD-MAE	✓					✓	93.5
MAE							95.7
SD-MAE		✓				✓	95.5

In order to validate the generalizability of our SD-MAE, we adopt the in-domain transfer protocol by crossing fine-tuning on the different datasets. As shown in Tab. 4, among most results, our SD-MAE achieves the higher performance. And we notice that MAE is better than our SD-MAE only when the pre-training datasets have smaller classes than the fine-tuning datasets (see red results).

3.5 Visualization

For investigating the effectiveness of joining self-distillation into MAE, we perform two evaluation of visualization. Firstly, we are curious about the results of image reconstruction. In Fig. 3, we present two recovering examples by using our SD-MAE. It is seen that slightly better reconstruction is obtained by SD-MAE compared to MAE. It demonstrates that self-distillation reinforces the learning capability of the MAE encoder.

And we also visualize the attention map of MAE and SD-MAE. As show in Fig. 4, we can clearly find that our SD-MAE is more focused compared to MAE. That is, SD-MAE can learn what is the most critical feature and make predictions based on that feature. This is the same way that a pathologist can

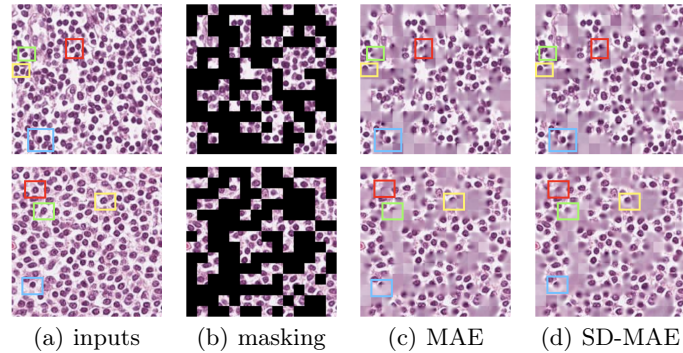


Fig. 3. Images reconstructed by MAE and SD-MAE on NCT-CRC. The color boxes highlight their details

determine the type of cancer based on only a few cells or a small part of an image. We attribute this phenomenon to the fact that self-distillation strengthens the ability of extracting features of encoder through the direct backpropagation of loss.

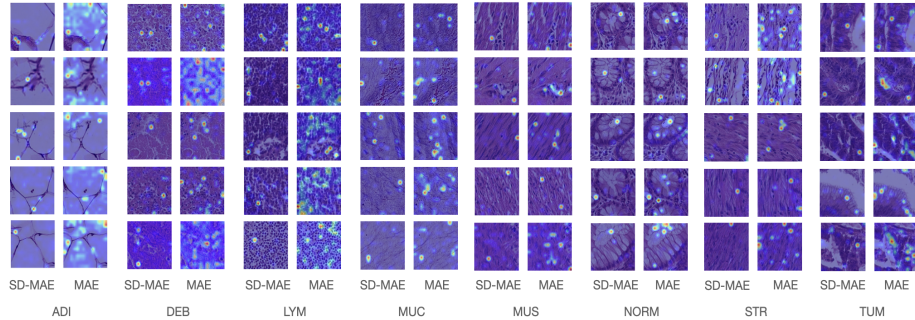


Fig. 4. We look at the attention map of the last layer of ViT after pre-training over the validation dataset of NCT-CRC. Note that the below words represent the different cancer classes.

4 Conclusion

We introduce MAE to pathological image classification and propose SD-MAE. We firstly empirically prove the effect of visible patches after decoding for pathological image classification. And secondly, a novel self-distillation scheme which transfers knowledge from the decoder to the encoder is developed to fully make use of these patches, guiding a more effective visual pre-training. Experimental

results on two pathological and visualization demonstrate the effectiveness of our SD-MAE, which would be a promising paradigm for pathological image analysis. In the future, we plan to evaluate our SD-MAE on other downstream tasks such as nuclei segmentation, etc.

References

1. Bao, H., Dong, L., Wei, F.: Beit: Bert pre-training of image transformers. arXiv preprint arXiv:2106.08254 (2021)
2. Bejnordi, B.E., Veta, M., Van Diest, P.J., Van Ginneken, B., Karssemeijer, N., Litjens, G., Van Der Laak, J.A., Hermsen, M., Manson, Q.F., Balkenhol, M., et al.: Diagnostic assessment of deep learning algorithms for detection of lymph node metastases in women with breast cancer. *Jama* **318**(22), 2199–2210 (2017)
3. Bejnordi, B.E., Veta, M., Van Diest, P.J., Van Ginneken, B., Karssemeijer, N., Litjens, G., Van Der Laak, J.A., Hermsen, M., Manson, Q.F., Balkenhol, M., et al.: Diagnostic assessment of deep learning algorithms for detection of lymph node metastases in women with breast cancer. *Jama* **318**(22), 2199–2210 (2017)
4. Bejnordi, B.E., Veta, M., Van Diest, P.J., Van Ginneken, B., Karssemeijer, N., Litjens, G., Van Der Laak, J.A., Hermsen, M., Manson, Q.F., Balkenhol, M., et al.: Diagnostic assessment of deep learning algorithms for detection of lymph node metastases in women with breast cancer. *Jama* **318**(22), 2199–2210 (2017)
5. Caron, M., Touvron, H., Misra, I., Jégou, H., Mairal, J., Bojanowski, P., Joulin, A.: Emerging properties in self-supervised vision transformers. In: Proceedings of the IEEE/CVF International Conference on Computer Vision. pp. 9650–9660 (2021)
6. Chen, T., Kornblith, S., Norouzi, M., Hinton, G.: A simple framework for contrastive learning of visual representations. In: International conference on machine learning. pp. 1597–1607. PMLR (2020)
7. Chen, X., Xie, S., He, K.: An empirical study of training self-supervised vision transformers. arXiv preprint arXiv:2104.02057 (2021)
8. Ciga, O., Xu, T., Martel, A.L.: Self supervised contrastive learning for digital histopathology. *Machine Learning with Applications* **7**, 100198 (2022)
9. Devlin, J., Chang, M.W., Lee, K., Toutanova, K.: Bert: Pre-training of deep bidirectional transformers for language understanding. arXiv preprint arXiv:1810.04805 (2018)
10. Grill, J.B., Strub, F., Altché, F., Tallec, C., Richemond, P.H., Buchatskaya, E., Doersch, C., Pires, B.A., Guo, Z.D., Azar, M.G., et al.: Bootstrap your own latent: A new approach to self-supervised learning. arXiv preprint arXiv:2006.07733 (2020)
11. He, K., Chen, X., Xie, S., Li, Y., Dollár, P., Girshick, R.: Masked autoencoders are scalable vision learners. arXiv preprint arXiv:2111.06377 (2021)
12. Hinton, G., Vinyals, O., Dean, J.: Distilling the knowledge in a neural network (2015)
13. Kather, J.N.: Histological images for MSI vs. MSS classification in gastrointestinal cancer, FFPE samples (Feb 2019). <https://doi.org/10.5281/zenodo.2530835>, <https://doi.org/10.5281/zenodo.2530835>
14. Kather, J.N., Krisam, J., Charoentong, P., Luedde, T., Herpel, E., Weis, C.A., Gaiser, T., Marx, A., Valous, N.A., Ferber, D., et al.: Predicting survival from colorectal cancer histology slides using deep learning: A retrospective multicenter study. *PLoS medicine* **16**(1), e1002730 (2019)

15. Liu, X., Zhang, F., Hou, Z., Mian, L., Wang, Z., Zhang, J., Tang, J.: Self-supervised learning: Generative or contrastive. *IEEE Transactions on Knowledge and Data Engineering* (2021)
16. Pathak, D., Krahenbuhl, P., Donahue, J., Darrell, T., Efros, A.A.: Context encoders: Feature learning by inpainting. In: *Proceedings of the IEEE conference on computer vision and pattern recognition*. pp. 2536–2544 (2016)
17. Stacke, K., Unger, J., Lundström, C., Eilertsen, G.: Learning representations with contrastive self-supervised learning for histopathology applications. *arXiv preprint arXiv:2112.05760* (2021)
18. Taleb, A., Lippert, C., Klein, T., Nabi, M.: Multimodal self-supervised learning for medical image analysis. In: *International Conference on Information Processing in Medical Imaging*. pp. 661–673. Springer (2021)
19. Trockman, A., Kolter, J.Z.: Patches are all you need? (2022)
20. Wang, X., Yang, S., Zhang, J., Wang, M., Zhang, J., Huang, J., Yang, W., Han, X.: Transpath: Transformer-based self-supervised learning for histopathological image classification. In: *International Conference on Medical Image Computing and Computer-Assisted Intervention*. pp. 186–195. Springer (2021)
21. Wei, C., Fan, H., Xie, S., Wu, C.Y., Yuille, A., Feichtenhofer, C.: Masked feature prediction for self-supervised visual pre-training. *arXiv preprint arXiv:2112.09133* (2021)
22. Xie, X., Chen, J., Li, Y., Shen, L., Ma, K., Zheng, Y.: Instance-aware self-supervised learning for nuclei segmentation (2020)
23. Xie, Z., Zhang, Z., Cao, Y., Lin, Y., Bao, J., Yao, Z., Dai, Q., Hu, H.: Simmim: A simple framework for masked image modeling. *arXiv preprint arXiv:2111.09886* (2021)
24. Yan, R., Ren, F., Wang, Z., Wang, L., Ren, Y., Liu, Y., Rao, X., Zheng, C., Zhang, F.: A hybrid convolutional and recurrent deep neural network for breast cancer pathological image classification. In: *2018 IEEE International Conference on Bioinformatics and Biomedicine (BIBM)*. pp. 957–962. IEEE (2018)
25. Yang, P., Hong, Z., Yin, X., Zhu, C., Jiang, R.: Self-supervised visual representation learning for histopathological images. In: *International Conference on Medical Image Computing and Computer-Assisted Intervention*. pp. 47–57. Springer (2021)
26. Zhang, L., Song, J., Gao, A., Chen, J., Bao, C., Ma, K.: Be your own teacher: Improve the performance of convolutional neural networks via self distillation (2019)
27. Zhuang, X., Li, Y., Hu, Y., Ma, K., Yang, Y., Zheng, Y.: Self-supervised feature learning for 3d medical images by playing a rubik’s cube. In: *International Conference on Medical Image Computing and Computer-Assisted Intervention*. pp. 420–428. Springer (2019)